

The Formation of a Forward-Tilting Cold Front with Multiple Cloud Bands during Superstorm 1993

DAVID M. SCHULTZ

NOAA/National Severe Storms Laboratory, Norman, Oklahoma

W. JAMES STEENBURGH

NOAA Cooperative Institute for Regional Prediction, and Department of Meteorology, University of Utah, Salt Lake City, Utah

(Manuscript received 8 January 1998, in final form 8 June 1998)

ABSTRACT

A mesoscale-model simulation is used to examine the evolution of the cold front and accompanying cloud bands in eastern Mexico associated with Superstorm 1993 (12–14 March). The simulated cold front differed in structure and evolution from a classical cold front, in agreement with evidence from observations and European Centre for Medium-Range Weather Forecasts analyses. The surface cold front, as defined by the leading edge of strong northerlies and cold advection, initially possessed a rearward tilt with height over southern Texas. Within 6 h, the leading edge of the front moved equatorward and developed a large-scale forward tilt of greater than 200 km in the horizontal from the surface to 700 hPa. This forward tilt occurred as a mid- to upper-tropospheric baroclinic zone arrived from over the Sierra Madre, descended into eastern Mexico, and interacted with the surface cold front. Embedded within this large-scale forward tilt was a locally enhanced horizontal potential temperature gradient that also tilted forward ~100 km from the surface to 850 hPa. Tilting frontogenesis associated with ascent at the leading edge of the surface front was responsible for the smaller-scale forward-tilting structure. This surface-based ascent is believed to have caused the primary cloud band observed from satellite imagery that is coincident with the leading edge of the front, whereas a second region of ascent, elevated at the leading edge of the mid- to upper-tropospheric baroclinic zone, is believed to have caused the prefrontal cloud band revealed by satellite imagery. Subsidence behind the forward-tilting cold-frontal structure at and above 850 hPa (and concomitant divergence underneath) resulted in frontolysis of the surface front, and eventually the dissipation of the primary cloud band, leading to the dominance of the prefrontal cloud band. Finally, the Superstorm 1993 cold front is compared and contrasted to nonclassical cold-frontal structures found in the literature and a general context for frontal interaction is discussed.

1. Introduction

The classical conceptual model of a cold front, as derived from case studies of observed events (e.g., Sanders 1955; Shapiro 1984; Bond and Fleagle 1985; Bond and Shapiro 1991; Neiman et al. 1991) and as summarized in review articles (e.g., Keyser 1986; Browning 1990), typically is manifested as a baroclinic zone that monotonically tilts rearward with height over the cold postfrontal air. At the leading edge of the cold front, a narrow band of ascent occurs that sometimes produces a rope cloud (e.g., Janes et al. 1976; Shapiro and Keyser 1990, section 10.3.1), and, if precipitating, a narrow cold-frontal rainband (e.g., Browning and Har-

rold 1970; Knight and Hobbs 1988). The passage of a classical cold front at the surface typically is marked by a relative minimum in sea level pressure (pressure trough), cyclonic wind shift, and temperature decrease (e.g., Bluestein 1993, 256–269). In some cases, however, cold fronts do not possess these characteristics; they can be tilted forward with height, possess prefrontal features (e.g., troughs, cloud bands), or both.

Forward-tilting cold fronts¹ have been noted previ-

Corresponding author address: Dr. David M. Schultz, NOAA/National Severe Storms Laboratory, 1313 Halley Circle, Norman, OK 73069.
E-mail: schultz@nssl.noaa.gov

¹ In this paper, the term *forward-tilting cold front* is used to describe a cold front where the onset of cold advection in the lower- to midtroposphere precedes that at the surface. A possible interpretation of this definition, and one that appeared to be in favor among meteorologists during the 1940s and 1950s (see, e.g., Berry et al. 1945, 653; Newton 1963, 36), is that a forward-tilting front may be associated with regions of the atmosphere that are absolutely unstable (i.e., $\partial\theta/\partial z < 0$), but this scenario is not validated by the case studies in the following discussion (section 1) and later in this paper (e.g., Fig. 6d and section 6).

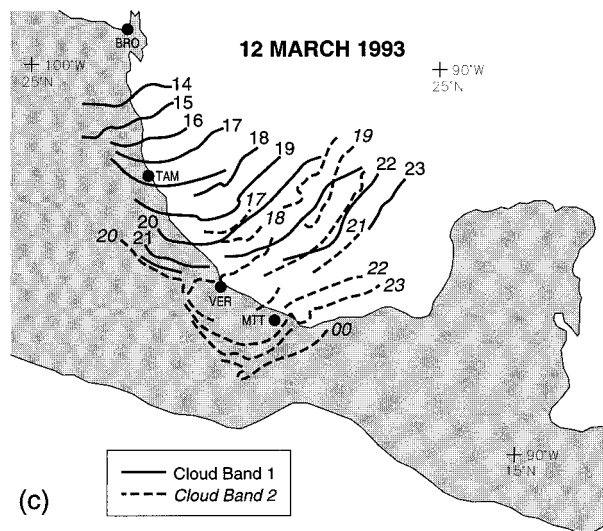
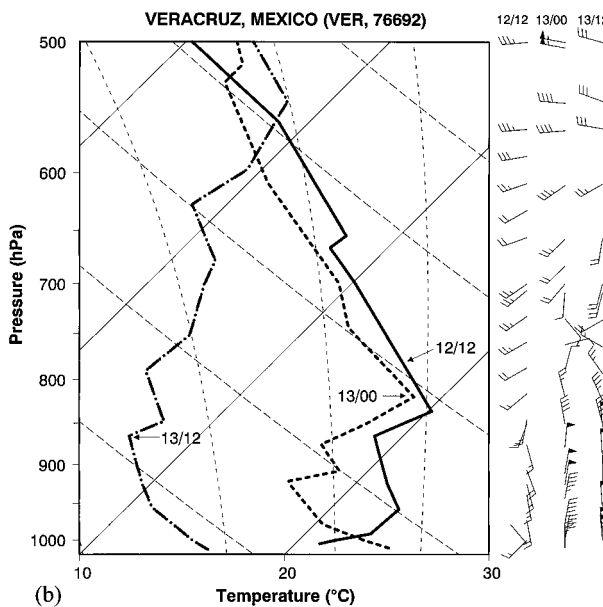
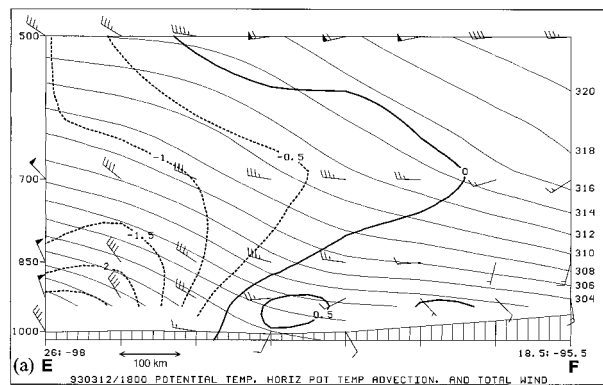


FIG. 1. (a) Cross section EF (location shown in Fig. 6a) from European Centre for Medium-Range Weather Forecasts analysis at 1800 UTC 12 March 1993: potential temperature (thin solid lines every 2 K), potential temperature advection [every 0.5 K h⁻¹; negative

ously in the literature. Brunt (1934, 344–345) claimed that there is “definite observational evidence” of cold fronts having a “nose” (a forward protrusion of unspecified length) as high as 500 m above ground. Brunt also argued that a surface pressure trough would be found below the nose of the cold front (a prefrontal trough). Other early views of forward-tilting cold fronts can be found in Bjerknes (1930, Fig. 8) and Flower (1931). More recent observational (Hardy et al. 1973; Bedard and Sanders 1978; Morales 1981, Fig. 9; Locatelli et al. 1989) and numerical modeling (Kuo and Reed 1988; Mass and Schultz 1993; Steenburgh and Mass 1994; Colle and Mass 1995) work has presented examples of fronts that are forward-tilting with height. Also, several authors have suggested that some midlatitude cold fronts entering the Tropics first arrive aloft and later become evident at the surface (e.g., Forsdyke 1949, 40; Palmer 1951, 867; Trewartha 1966, 46–48).

The existence of prefrontal features such as troughs, wind-shift lines, and cloud bands has also been recognized previously (e.g., Bjerknes 1930, 5–7; Tepper 1950; Newton 1950; Garratt 1988; Hanstrum et al. 1990a, b; Bluestein 1993, 258–259; Charney and Fritsch 1996; Browning et al. 1997; Neiman et al. 1998; Bryan and Fritsch 1998; Sanders 1998). Sanders (1983), Colle and Mass (1995), Sanders and Doswell (1995), and Hutchinson and Bluestein (1998) presented observational evidence that troughs and wind-shift lines can precede cold fronts in the southern and central United States. In fact, as many as 60% of the cold fronts in the lee of the Rocky Mountains may be associated with prefrontal wind shifts, often identified as lee troughs or drylines (Hutchinson and Bluestein 1998). Furthermore, prefrontal pressure troughs associated with midlatitude cold fronts entering the Tropics have been noted by several authors (e.g., Palmer 1951, 867; Trewartha 1966, 46; Fermor 1971; Hastenrath 1985, 241).

Schultz et al. (1997) performed an observational case study of the midlatitude cold front associated with Superstorm 1993 (12–14 March; hereafter SS93) that moved equatorward into the Tropics along the eastern slopes of the Sierra Madre of Mexico and Central America. They found that the structure and evolution of the cold front in eastern Mexico was nonclassical in two important aspects: the cold-frontal structure appeared to be forward tilting, and prefrontal troughs/cloud bands

(positive and zero) values dashed (solid) represent cold (warm) advection], and winds (one pennant, full barb, and half-barb denote 25, 5, and 2.5 m s⁻¹, respectively; displayed every 132 km). (b) Wind (one pennant, full barb, and half-barb denote 25, 5, and 2.5 m s⁻¹, respectively) and temperature (°C) profiles for Veracruz, Mexico, at 1200 UTC 12 March 1993 (12/12; solid line), 0000 UTC 13 March 1993 (13/00; dashed line), and 1200 UTC 13 March 1993 (13/12; dashed-dotted line). (c) Isochrones of cloud bands as determined from available visible and infrared satellite imagery. Isochrones of cloud band 1 (2) denoted by solid (dashed) lines; UTC hours labeled in normal typeface (*italics*). Adapted from Schultz et al. (1997, Fig. 10).

were present. Figure 1 presents evidence for these non-classical features. First, a cross section through the surface cold front from the European Centre for Medium-Range Weather Forecasts (ECMWF) analysis at 1800 UTC 12 March 1993 indicates that the cold advection at 850–700 hPa occurred 200–300 km ahead of the cold advection at the surface (Fig. 1a; the location of cross section EF is shown in Figs. 6a,c). Second, the change in the lower-tropospheric temperature and wind profiles at Veracruz, Mexico (VER in Fig. 1c) between 1200 UTC 12 March and 0000 UTC 13 March suggests that, because of strong afternoon boundary layer mixing and surface heating, the strongest northerlies and largest temperature decrease arrived at 925–850 hPa before arriving at the surface (Fig. 1b), thereby suggesting a forward tilt to the front. Later (1200 UTC 13 March), the temperature and strong winds were more well mixed through the lowest 50–150 hPa (Fig. 1b). Finally, Schultz et al. (1997, Fig. 10) described multiple cloud bands that were associated with the cold front at different times during its evolution. In particular, the cold front, initially identified by a rope cloud (the *primary cloud band*; cloud band 1 in Fig. 1c), began with the pressure minimum, wind shift, and temperature decrease nearly coincident, characteristics similar to a classical cold front. By 1700 UTC 12 March, a second cloud band (the *prefrontal cloud band*; cloud band 2 in Fig. 1c) formed in advance of the primary cloud band and was associated with a prefrontal pressure trough.² Over the next 5 h, the surface wind in between the two cloud bands increased in magnitude and became increasingly northerly, as if the interstitial air were being diluted by higher-momentum northerlies from aloft (Schultz et al. 1997, 23–24). By 2200 UTC 12 March, cloud band 2 became the leading edge of the surface cold front and cloud band 1 was dissipating (Fig. 1c).

The purpose of this paper is to address these non-classical aspects of the cold front associated with SS93 (the forward tilt of the cold front and its associated cloud bands) as it moved equatorward along the eastern slopes of the Sierra Madre in Mexico. The observed data presented in Schultz et al. (1997), although suggestive, was often inadequate to provide additional details about the evolution of this case and, therefore, to ascertain more confidently its structure and dynamics. Consequently, a mesoscale model simulation is used to provide a high-resolution four-dimensional dataset for analysis and diagnosis. The mesoscale model and its configuration for this study are described in section 2. The structure and evolution of the simulated cold front are presented in section 3. In sections 4 and 5, the model simulation is further studied through trajectory and frontogenesis diagnostics, respectively, in order to examine the for-

mation and maintenance of the forward tilt to the cold-frontal structure and the evolution of the prefrontal and primary cloud bands. Finally, in section 6, we compare and contrast the SS93 cold front to other frontal structures in the literature.

2. Mesoscale-model description

The Pennsylvania State University–National Center for Atmospheric Research mesoscale model (PSU-NCAR MM5), a nonhydrostatic, primitive equation, σ -coordinate model (Dudhia 1993; Grell et al. 1994), was employed to simulate the SS93 cold front. The simulation featured two domains with horizontal resolutions of 60 and 20 km (Fig. 2), nested with a two-way interactive mesh-refinement scheme. Thirty variably spaced half- σ levels³ were used with vertical resolution varying from approximately 10 hPa in the boundary layer to approximately 50 hPa in the upper troposphere. Precipitation processes were parameterized using a mixed-phase explicit-moisture scheme that includes prognostic equations for water vapor, cloud water, rainwater, cloud ice, and snow and also allows for supercooled water droplets. The Kain–Fritsch cumulus parameterization (Kain and Fritsch 1993) was used to represent subgrid-scale convective precipitation. Other parameterizations included a multilevel planetary boundary layer (Zhang and Anthes 1982), a long- and shortwave atmospheric radiation scheme (Dudhia 1989), and a radiative upper boundary condition (Klemp and Durran 1983). Further information about the model terrain and initialization can be found in Steenburgh et al. (1998, section 3). Throughout this paper, only output from the 20-km domain is displayed, with the forecast hour of the simulation defined relative to the beginning of the 12-h dynamic-initialization period at 0000 UTC 12 March (0 h).

3. Synoptic evolution

Our analysis of the cold-frontal structure focuses on eastern Mexico for three reasons. First, cloud bands 1 and 2 (nearly two-dimensional over a length of 200–300 km), the features we wish to diagnose, occur only in eastern Mexico and near the coast (Fig. 1c). Second, numerous cross sections (not shown) indicate that the forward-tilting structure is unique to eastern Mexico. That the forward-tilt is found in the same region as the cloud bands suggests that the two features may be related. Third, the surface and upper-air observations for validation with the mesoscale-model simulation are most abundant in eastern Mexico.

² Cloud bands 3–5 are not discussed in this paper. The dynamics associated with cloud band 5 over the Gulf of Tehuantepec is examined by Steenburgh et al. (1998).

³ Specifically, the half- σ levels were located at $\sigma = 0.995, 0.985, 0.970, 0.945, 0.915, 0.885, 0.855, 0.825, 0.795, 0.765, 0.735, 0.705, 0.675, 0.645, 0.615, 0.585, 0.550, 0.510, 0.470, 0.430, 0.390, 0.350, 0.310, 0.270, 0.230, 0.190, 0.150, 0.110, 0.070, 0.025$.

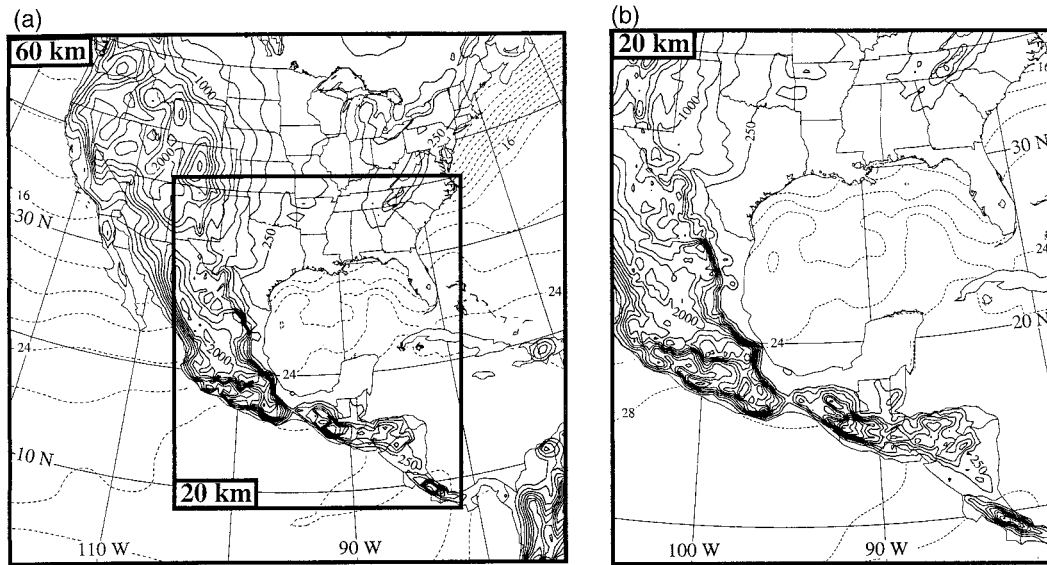


FIG. 2. PSU-NCAR MM5 domains, topography (solid lines every 250 m, starting at 250 m), and sea surface temperature (dashed lines every 2°C).

To illustrate the large-scale environment in eastern Mexico shortly after the initiation of the cold surge, surface, 850-hPa, and 500-hPa analyses for 12 h into the simulation (1200 UTC 12 March 1993) are presented in Figs. 3a–c. The simulated surface cyclone was located southeast of Brownsville, Texas (BRO in Fig. 1c) and the leading edge of the surface cold front⁴ was located just south of the Texas–Mexico border with 10 m s^{-1} northerlies yielding cold advection over south-central Texas (Fig. 3a). Note that the cyclogenesis was occurring south of the primary baroclinic zone over the Gulf of Mexico and the thermal gradient south of the analyzed cold front, laid down by prior convection in the area, was characterized by warm advection (Fig. 3a). At this time, the lower-tropospheric cold front was rearward sloping as the leading edge of strong cold advection at the surface (near BRO) was about 200 km farther equatorward than at 850 hPa (cf. Figs. 3a,b). The rearward tilt is further illustrated by cross section AB (Fig. 3d; the location is shown in Figs. 3a,c), oriented nearly perpendicular to the surface front. Cross section AB shows the leading edge of the cold advection (identified by the thick solid line labeled 0) tilting rearward from the surface to 850 hPa, roughly coincident with the bar-

oclinicity and wind shift from southerly–southwesterly to northerly–northeasterly. At 500 hPa (Fig. 3c), a region of strong winds and cold advection was found over northeastern Mexico in association with the upper-tropospheric disturbance responsible for the initial SS93 cyclogenesis over the Gulf of Mexico [associated with the so-called potential vorticity anomaly C , as illustrated in Bosart et al. (1996, Fig. 3) and Dickinson et al. (1997, Fig. 3)]. Cross section CD, taken across the 500-hPa baroclinic zone (Fig. 4; the location is shown in Figs. 3a,c), illustrates that the baroclinicity extended from the tropopause through the midtroposphere down to about 800 hPa. Hereafter, we will refer to this baroclinic zone as the *mid- to upper-tropospheric baroclinic zone*. At this time, the mid- to upper-tropospheric baroclinic zone was further equatorward than the surface baroclinic zone, which, in cross section CD (Fig. 4), was trapped against the northeast slopes of the Sierra Madre (see also the surface potential temperature in Fig. 3a). In cross section AB (Fig. 3d), this mid- to upper-tropospheric baroclinic zone was associated with cold advection at 700–500 hPa, which preceded that at the surface by about 200 km. Low relative humidity air (indicative of a recent history of subsidence associated with the mid- to upper-tropospheric baroclinic zone, a point to be illustrated further in section 4) was found on the equatorward side of the mid- to upper-tropospheric baroclinic zone above 800 hPa (Fig. 3d). In general, these simulated analyses from the PSU-NCAR MM5 agree well with manual analyses for this same time (1200 UTC 12 March 1993) in Kocin et al. (1995, their Figs. 3d–f).

By 15 h (Fig. 5), cross section AB shows that the region of cold advection and drier air associated with

⁴ To distinguish between the leading edge of the surface cold front and the prefrontal pressure trough, the cold front is defined in this paper as the leading edge of strong northerlies and strong cold advection, consistent with the definition employed by Colle and Mass (1995, 2577) in their study of cold surges east of the Rocky Mountains. Because a purpose of this paper is to distinguish the prefrontal trough from the cold front, the definition employed presently is not consistent with the more liberal definition of Steenburgh et al. (1998), who placed the cold front coincident with the pressure trough and northerly wind shift.

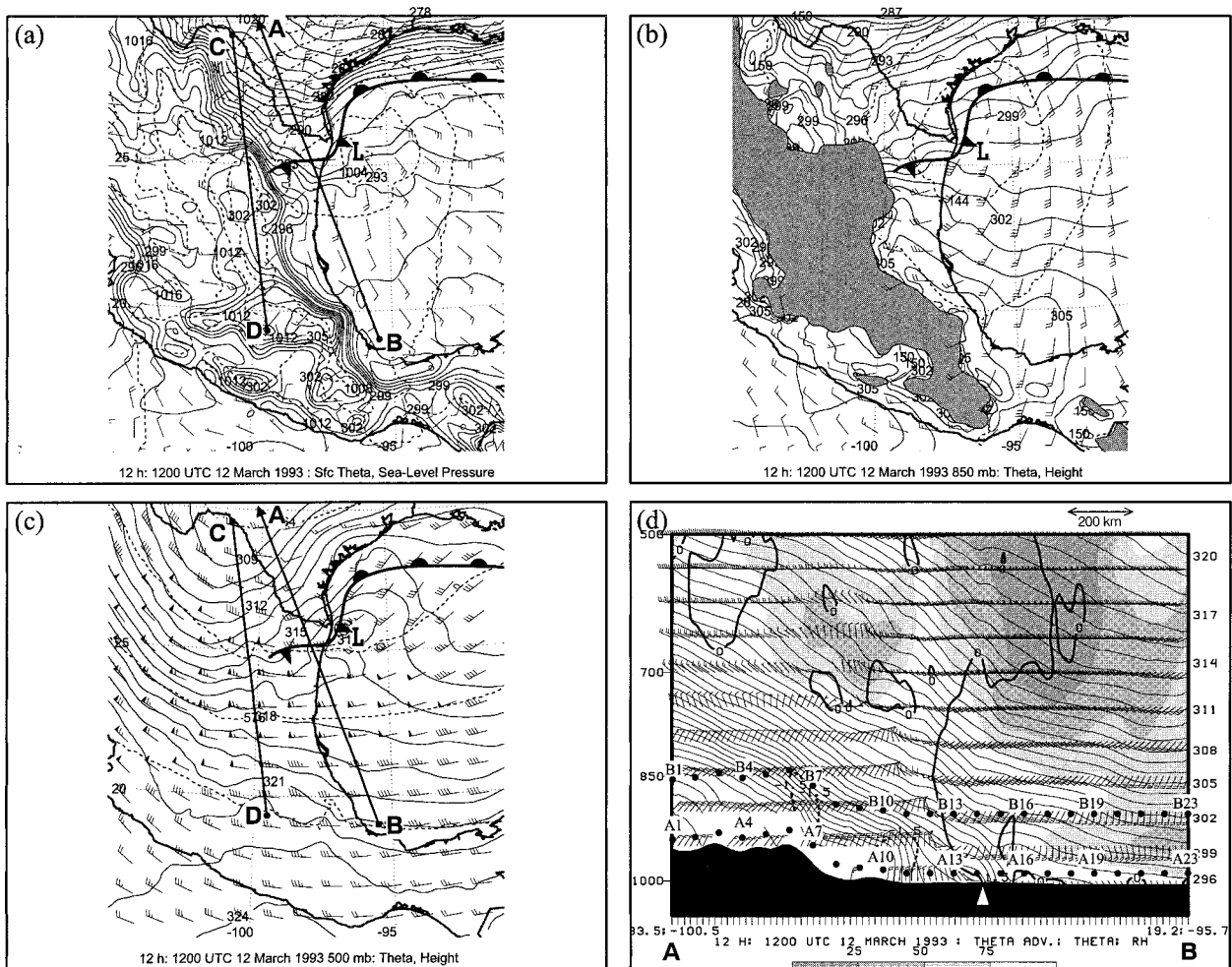


FIG. 3. Simulated analyses at 12 h (1200 UTC 12 March 1993). (a) Potential temperature at the lowest half- σ level ($\sigma = 0.995$; approximately 40 m above ground level) (thin solid lines every 1 K), sea level pressure (dashed lines every 2 hPa), and surface winds (one pennant, full barb, and half-barb denote 25, 5, and 2.5 m s⁻¹, respectively; every 120 km); the location of cross sections AB and CD shown by thick solid lines; large L indicates position of surface cyclone center; frontal symbols are conventional and represent surface frontal positions. (b) 850 hPa: potential temperature (thin solid lines every 1 K), geopotential height (dashed lines every 3 dam), and winds [as in (a)]. Areas with surface pressure less than 850 hPa are shaded; large L indicates position of surface cyclone center; frontal symbols are conventional and represent surface frontal positions. (c) 500 hPa: potential temperature (thin solid lines every 1 K), geopotential height (dashed lines every 6 dam), and winds [as in (a)]; the locations of cross sections AB and CD shown by thick solid lines; large L indicates position of surface cyclone center; frontal symbols are conventional and represent surface frontal positions. (d) Cross section AB [location shown in (a) and (c)]: potential temperature (thin solid lines every 1 K), relative humidity (% , shaded according to scale), potential temperature advection [every 1.5 K h⁻¹; negative (positive and zero) values dashed (solid) represent cold (warm) advection], and winds [as in (a); every 19 km]. Dots represent the ending locations of trajectories at 12 h in Fig. 10 (labeled every third dot, except A23 and B23). White triangle indicates surface location of cold front.

the mid- to upper-tropospheric baroclinic zone had descended to about 850 hPa. The nascent interaction of the mid- to upper-tropospheric baroclinic zone with the surface cold front resulted in an apparent forward-tilting cold-frontal structure from the surface to 700 hPa, with 850–700-hPa cold advection located equatorward of the surface frontal position.

From 12 to 18 h (1200 to 1800 UTC 12 March 1993), the simulated surface cyclone deepened 8 hPa and moved east-northeastward (cf. Figs. 3a and 6a), and by 18 h (Fig. 6a) resembled the manually produced surface

analysis in Schultz et al. (1997, Fig. 13). At this time, the leading edge of the cold air at the surface was located near Tampico, Mexico (TAM in Fig. 1c), with the leading edge of cold advection at 850–700 hPa overspreading that at the surface by 200–300 km (cf. Figs. 6a,b). The horizontal potential temperature gradient within this region of forward tilt was approximately 1–2 K (100 km)⁻¹. Within this larger region of forward-tilting cold advection (hereafter referred to as the *large-scale forward tilt* of the cold front), a region of locally enhanced horizontal potential temperature gradient of 4–5 K (100

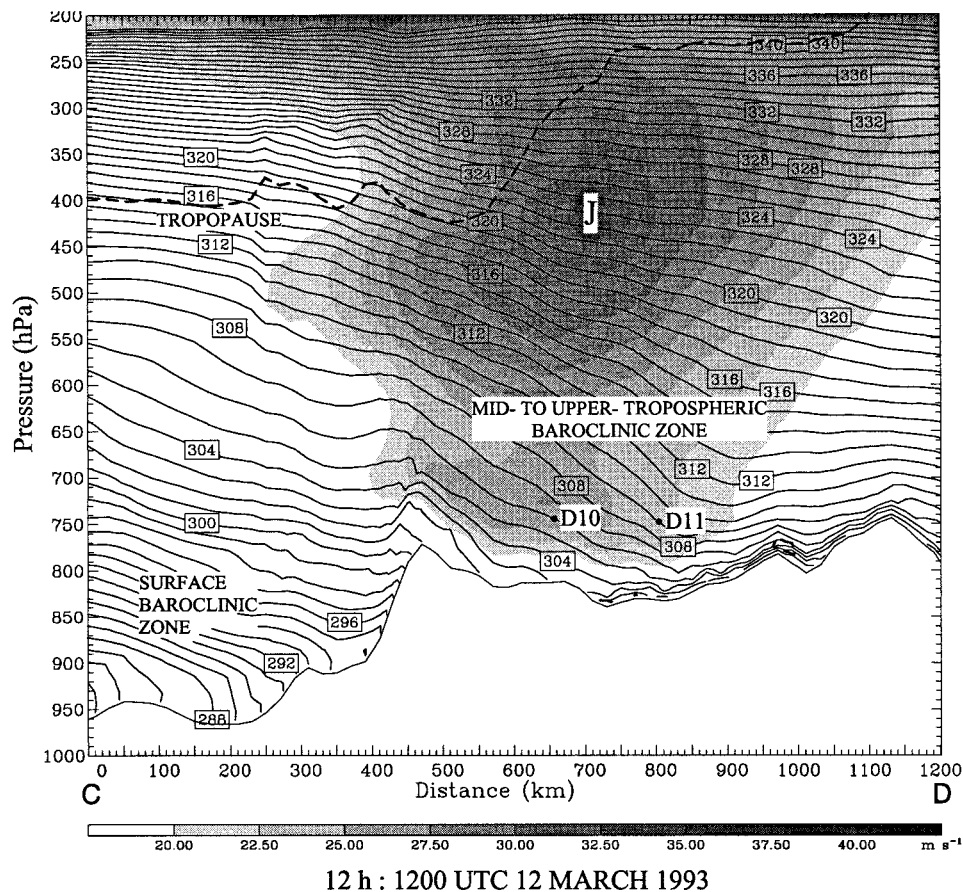


FIG. 4. Cross section CD (location shown in Figs. 3a,c) at 12 h (1200 UTC 12 March 1993): potential temperature (solid lines every 1 K), wind speed (m s^{-1} , shaded according to scale), and 1.5 potential vorticity unit ($1.5 \times 10^{-6} \text{ m}^2 \text{ s}^{-1} \text{ K kg}^{-1}$) contour (dashed line). Labeled dots (D10, D11) represent the approximate starting locations of trajectories at 12 h (trajectory paths shown in Fig. 11b). The location labeled J represents the total wind speed maximum.

km^{-1} was embedded (hereafter, the *small-scale forward tilt* of the cold front). This small-scale forward tilt of strong cold advection (as evinced by the -1.5 and -3 K h^{-1} contours) occurred from the surface to 850 hPa, with a forward tilt over this depth of about 100 km (Fig. 6d). Whereas the larger-scale forward tilt was due to the interaction between the mid- to upper-tropospheric baroclinic zone and the surface cold front, the embedded smaller-scale forward tilt was due to frontogenetical tilting by ascent from the surface cold front of the overlying baroclinicity (discussed further in section 5). Although much of the region immediately above the leading edge of the surface cold front became nearly isentropic from the surface to 850 hPa within this region of small-scale forward tilt (individual isentropes in this region were nearly vertical through a depth of about 200 hPa), absolute instability did not appear to develop in the model simulation (Fig. 6d; recall footnote 1). Indeed, such superadiabatic layers are removed by the model parameterization (Grell et al. 1994, 44). As evidence of a relationship between the forward tilt to the cold front and

the cloud bands discussed by Schultz et al. (1997), the locations of the observed primary cloud band (cloud band 1) and the prefrontal cloud band (cloud band 2) were similar to the leading edge of strong cold advection at the surface and 850 hPa, respectively (cf. Figs. 1c and 6a,b). This relationship between the cloud bands and the forward-tilting frontal structure will be discussed further in section 5. The 500-hPa trough and baroclinicity moved eastward (Fig. 6c) such that the most equatorward extent of the 500-hPa cold advection was 100 km poleward of the 850-hPa cold advection (Fig. 6b) and 250 km equatorward of the surface cold advection (see also Fig. 6d). In fact, the 850-hPa potential-temperature pattern was, in many ways, more similar to the 500-hPa potential-temperature pattern, indicating that the baroclinicity at 850 hPa may have been vertically continuous with the mid- to upper-tropospheric baroclinic zone (cf. Figs. 6b,c). This hypothesis is explored further in section 4.

At 21 h, the front continued to be tilted forward on

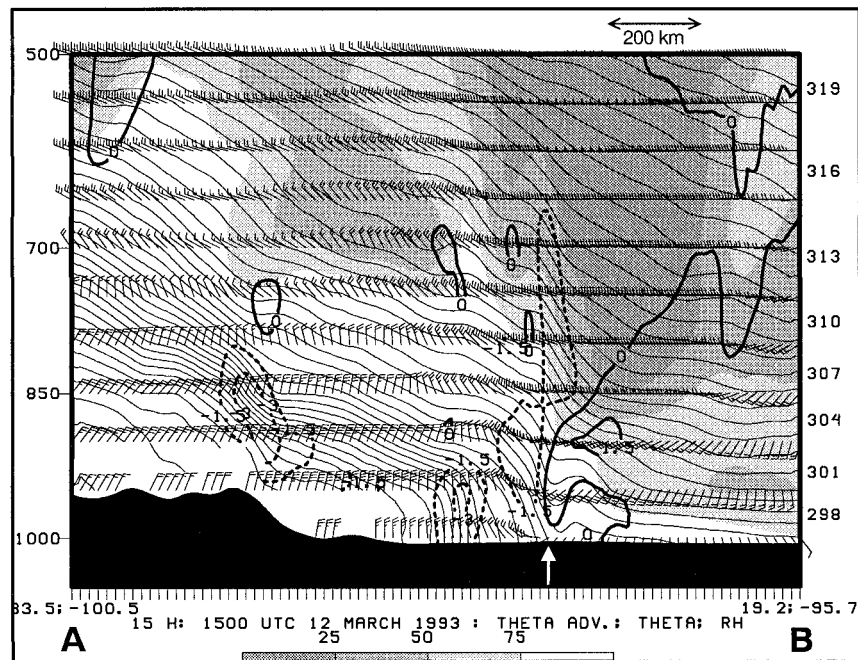


FIG. 5. Cross section AB (location shown in Figs. 3a,c) at 15 h (1500 UTC 12 March 1993): potential temperature (thin solid lines every 1 K), relative humidity (%), potential temperature advection [every 1.5 K h⁻¹; negative (positive and zero) values dashed (solid) represent cold (warm) advection], and winds (one pennant, full barb, and half-barb denote 25, 5, 2.5 m s⁻¹, respectively; every 19 km). White arrow indicates surface location of cold front.

both the large and small scales as shown in cross section EJ (Fig. 7; the location of which is shown in Fig. 6a). The prefrontal surface northerlies extended about 200 km ahead of the leading edge of the surface cold advection. It may be that the mixing down of air with higher northerly momentum from aloft in the region of the small-scale forward tilt is enhanced in this case because of its arrival into Mexico during the late afternoon, a time when mixing in the planetary boundary layer would be more vigorous. A similar process was discussed by Steenburgh and Mass (1994, 2753).

By 24 h (0000 UTC 13 March 1993; Fig. 8), the leading edge of the surface baroclinicity, preceded by surface northerlies and the prefrontal trough, was located just poleward of the Isthmus of Tehuantepec (Fig. 8a). The prefrontal onshore surface northerlies helped push the sea-breeze front inland along the north coast of the Isthmus of Tehuantepec (Figs. 8a,d). At 850 hPa, the potential temperature gradient along the leading edge had weakened (Fig. 8b), whereas at 500 hPa, the region of strongest cold advection had moved into the west-central Gulf of Mexico (Fig. 8c). The structure of the front is illustrated in cross section GH (Fig. 8d). Amplification of mountain waves over the isthmus occurred, disrupting the frontal structure at 700–900 hPa (Fig. 8d). Nevertheless, the leading edge of the cold advection tended to tilt rearward with height, returning to a more classical cold-frontal structure (supported by trajectories, presented in section 4).

To validate the simulated structure of the cold front and to illustrate the surface weather patterns associated with the passage of a forward-tilting front, observed and simulated time series at VER are presented in Fig. 9. The observed time series show a minimum in altimeter setting (i.e., a pressure check) indicating the passage of a pressure trough associated with cloud band 2 at 1845 UTC and an inflection in altimeter setting (superimposed upon a larger-scale pressure rise) indicating the passage of a pressure trough associated with cloud band 1 at 2130 UTC (Fig. 9a; Schultz et al. 1997, 22). The model-generated time series of sea level pressure at VER (Fig. 9a) exhibits a minimum at 19 h that represented the arrival of the prefrontal trough associated with the cloud band 2. Also associated with the passage of this trough in the model were decreasing 850-hPa temperature and increasing 850-hPa wind speed (Figs. 9b,c), providing additional evidence that the passage of cloud band 2 was followed by the onset of 850-hPa cold advection. The model-generated time series at VER exhibits the passage of a second feature after 22 h when the sea level pressure began to rise at an increased rate exceeding 1 hPa h⁻¹, the surface temperature began to decrease sharply, and the surface wind speed increased to 10–15 m s⁻¹ (Figs. 9a–c). These weather features represent the arrival at VER of the leading edge of the surface cold front (and cloud band 1) in the model. Except for a 1–2 hPa error in the pressure trough as-

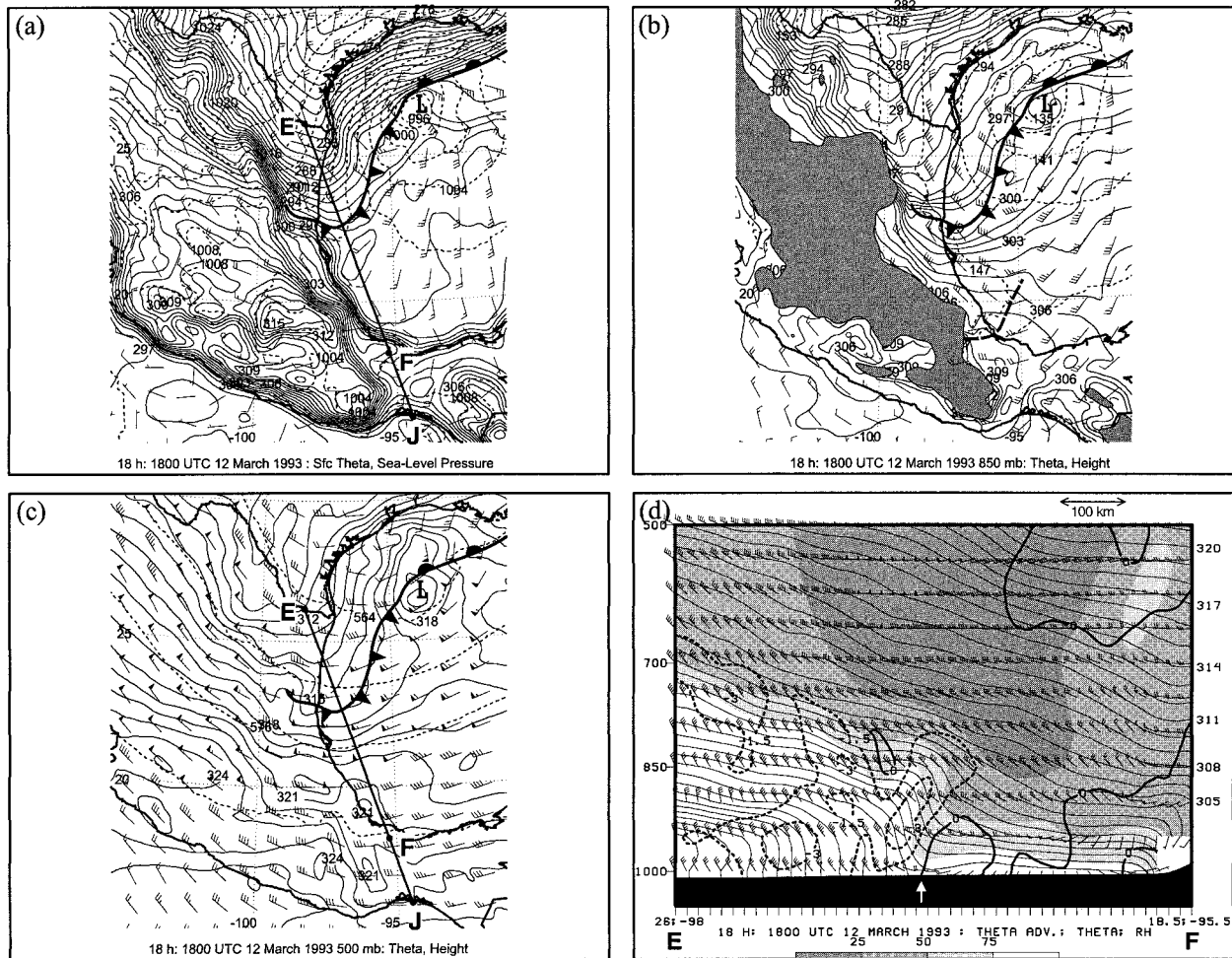


FIG. 6. As in Fig. 3 except for 18 h (1800 UTC 12 March 1993), location of cross section EF in (d) shown by thick solid line labeled EF in (a) and (c), and winds every 20 km in (d). Thick dashed line in (b) represents leading edge of strong 850-hPa cold advection.

sociated with the passage of cloud band 1 and a near-constant displacement between the observed altimeter and model pressure traces, the observed and modeled pressure traces between 1500 UTC 12 March and 0200 UTC 13 March (15 and 26 h) were broadly similar (Fig. 9a). The surface temperature and wind evolutions also seem to be well simulated, but the intensity of the peak temperatures and winds were underforecast (Figs. 9b,c).

Whereas the model-generated VER time series (Fig. 9) suggest that the previously discussed weather features associated with the passage of cloud bands 1 and 2 were reasonably simulated, the model-generated cloud-water fields (not shown) do not indicate the formation of these multiple cloud bands. As will be seen in section 5, however, regions of mesoscale ascent do occur in the simulation in nearly the correct locations as the expected cloud bands. Consequently, the appearance of these regions of ascent indicates that the dynamics to generate the cloud bands were present in the model.

4. Trajectory analysis

Results from the previous section indicate that the mesoscale-model simulation was able to develop the forward tilt to the cold front suggested by the observations. Also, this forward tilt appeared to be composed of a large-scale component (greater than 200 km over a depth from the surface to 700 hPa) and a small-scale component (around 100 km over a depth from the surface to 850 hPa). Evidence indicates that the forward-tilting cold-frontal structure resulted from the interaction of the mid- to upper-tropospheric baroclinic zone and the surface cold front. In this section three-dimensional air-parcel trajectories are computed to determine the source of the air at different levels in the cold-frontal structure, thereby confirming that the forward tilt was due to the frontal interaction. Trajectories, describing the airflow at 12 h, before the forward-tilting structure developed, and at 21 h, after the forward-tilting structure developed, demonstrate how the airflow changed over

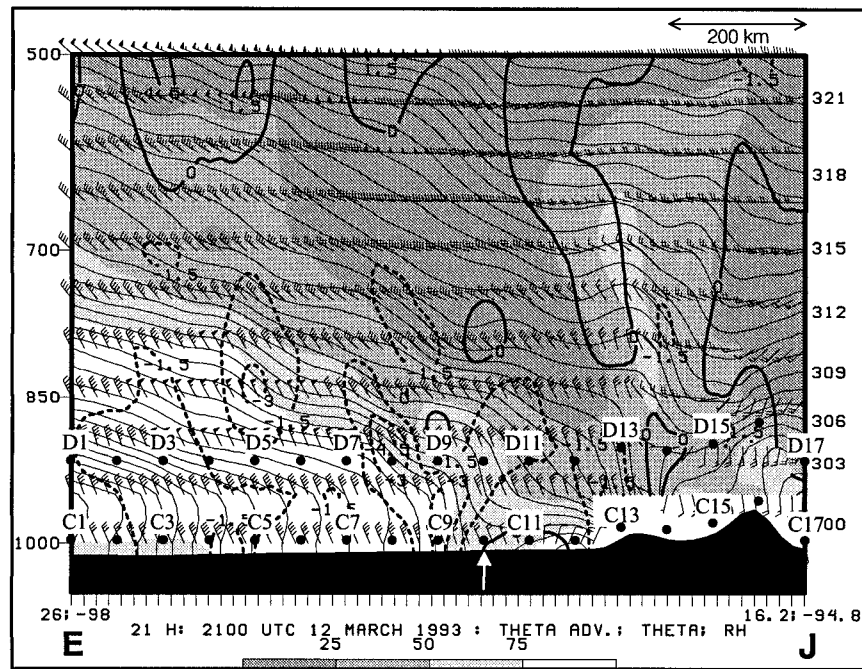


FIG. 7. As in Fig. 5 except at 21 h (2100 UTC 12 March 1993) and for cross section EJ (location shown in Figs. 6a,c); winds every 20 km in (d). Dots represent the ending locations of trajectories at 21 h in Fig. 11 (labeled every other dot).

time to create the forward-tilting structure. The trajectories were calculated from 60-min model-output files with a 15-min time step, using the approach described by Seaman (1987). The ending points at 12 and 21 h for the 9-h backward trajectories are displayed on cross sections (Figs. 3d and 7, respectively), nearly perpendicular to the surface cold front.

Nine-hour trajectories beginning at 3 h (0300 UTC 12 March 1993) and ending on $\sigma = 0.995$ (approximately 40 m above ground level) at 12 h (1200 UTC 12 March 1993) (Fig. 10a; trajectory ending locations are shown in Fig. 3d) show two airstreams: those poleward of the surface cold front moving southwestward (trajectories A1–A11) and those equatorward of the front moving northwestward (trajectories A14–A23). Trajectories A12–A13 started in the prefrontal air and were ingested into the postfrontal air in a manner similar to that described by Schultz and Mass (1993, 929). Trajectories ending on $\sigma = 0.885$ (approximately 850–914 hPa; note that trajectories labeled *Ann* and *Bnn* end at the same horizontal position) (Fig. 10b) show that the boundary between the two airstreams occurred between trajectories B11 and B13, with trajectory B12 having been ingested into the frontal zone, consistent with the cross section at this time (Fig. 3d). Therefore, at 12 h, trajectories in the lower troposphere indicate that the airstream boundary composing the front, consistent with the thermal structure from the cross section (Fig. 3d), tilted rearward with height.

By 21 h (2100 UTC 12 March 1993), the frontal

interaction had occurred with the cold front developing its large-scale and small-scale forward-tilting structure (Fig. 7). For the 9-h trajectories beginning at 12 h and ending on $\sigma = 0.995$ at 21 h (trajectory ending locations are shown in Fig. 7), trajectories C1–C8 originated and remained within the baroclinicity associated with the cold front (Fig. 11a). Trajectory C9 (see also Table 1) originated in the warm poleward flow ahead of the cold front, but between 17 and 18 h reached its most poleward position. After 18 h and the passage of the prefrontal trough, trajectory C9 turned equatorward, embedded in the prefrontal northerlies near the surface. After 19 h, the potential temperature of trajectory C9 began to drop (Table 1), indicating ingestion by the frontal zone. In contrast, trajectories C10–C13 appeared to reach their most poleward position around 19 h before turning and heading equatorward (Fig. 11a) without experiencing a decrease in potential temperature (not shown), indicating that trajectories C10–C13 were not ingested by the surface cold front (see also Fig. 7, where trajectories C10–C13 are found ahead of the surface position of the front). Therefore, the onset of equatorward motion of trajectories C9–C13 illustrated the passage of the prefrontal trough. Trajectories C14–C17 remained equatorward of the prefrontal trough.

Further aloft, 9-h trajectories D1–D17 ending on $\sigma = 0.885$ at 21 h are displayed in Fig. 11b (trajectory ending locations are shown in Fig. 7). Trajectories D1–D9 traveled within the baroclinicity behind the equatorward-moving cold front over southern Texas, as at

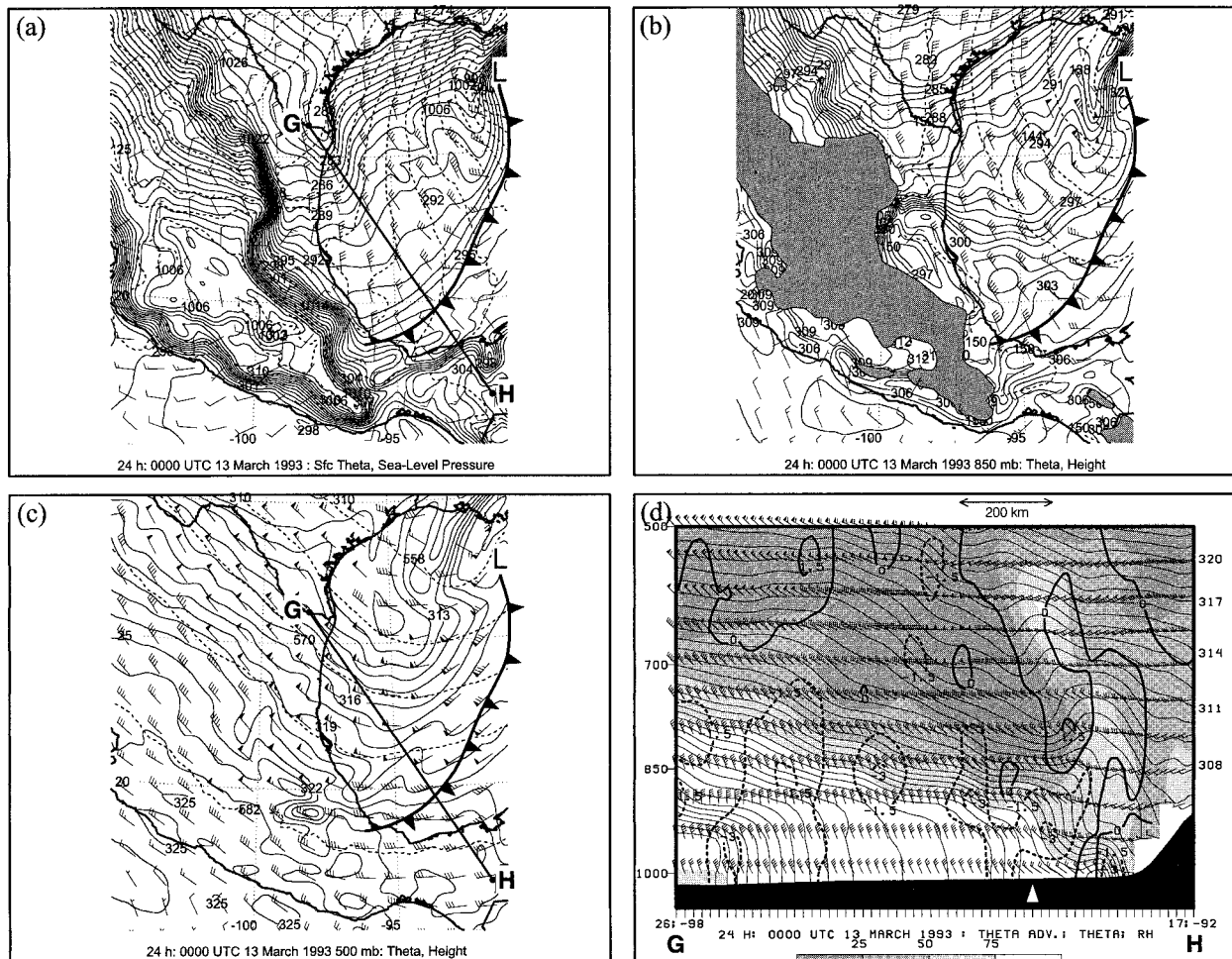


FIG. 8. As in Fig. 3 except at 24 h (0000 UTC 13 March 1993) and (d) cross section GH [location shown in (a) and (c)] and winds every 20 km.

12 h, whereas trajectories D14–D17 were found in the warm air equatorward of the front. Trajectories D10 and D11, however, both originated from the west in the baroclinicity associated with the mid- to upper-tropospheric baroclinic zone. The approximate positions of these two trajectories at 12 h are shown in Fig. 4. These two trajectories descended down the east side of the Sierra Madre and ended up in the forward-tilting portion of the cold front (Fig. 7). For example, trajectory D11 descended from 747 hPa to 901 hPa in 3 h (an average vertical velocity of $14 \mu\text{b s}^{-1}$). In contrast, trajectory D12, farther equatorward and not in the midtropospheric baroclinicity, underwent comparatively less descent (17 hPa compared to 154 hPa) over the same 3-h period. These descending trajectories help confirm that the forward-tilting front was formed by the interaction of the baroclinicity associated with the mid- to upper-tropospheric baroclinic zone arriving across the Sierra Madre and the surface cold front.

5. Frontogenesis analysis

To examine the strengthening and maintenance of the small-scale forward-tilting cold-frontal structure, we calculate frontogenesis, F . Originally defined by Petterssen (1936) for surface fronts, frontogenesis is the Lagrangian rate of change of the magnitude of the horizontal potential temperature (θ) gradient due to the horizontal wind. Miller (1948) extended Petterssen's definition to fronts in the free atmosphere by using the three-dimensional gradient of the potential temperature due to the three-dimensional wind. For this paper, we simplify Miller's form of F by calculating the frontogenesis of the *horizontal* potential temperature gradient due to the three-dimensional wind:

$$F = \frac{d}{dt} |\nabla_p \theta|, \tag{1}$$

where

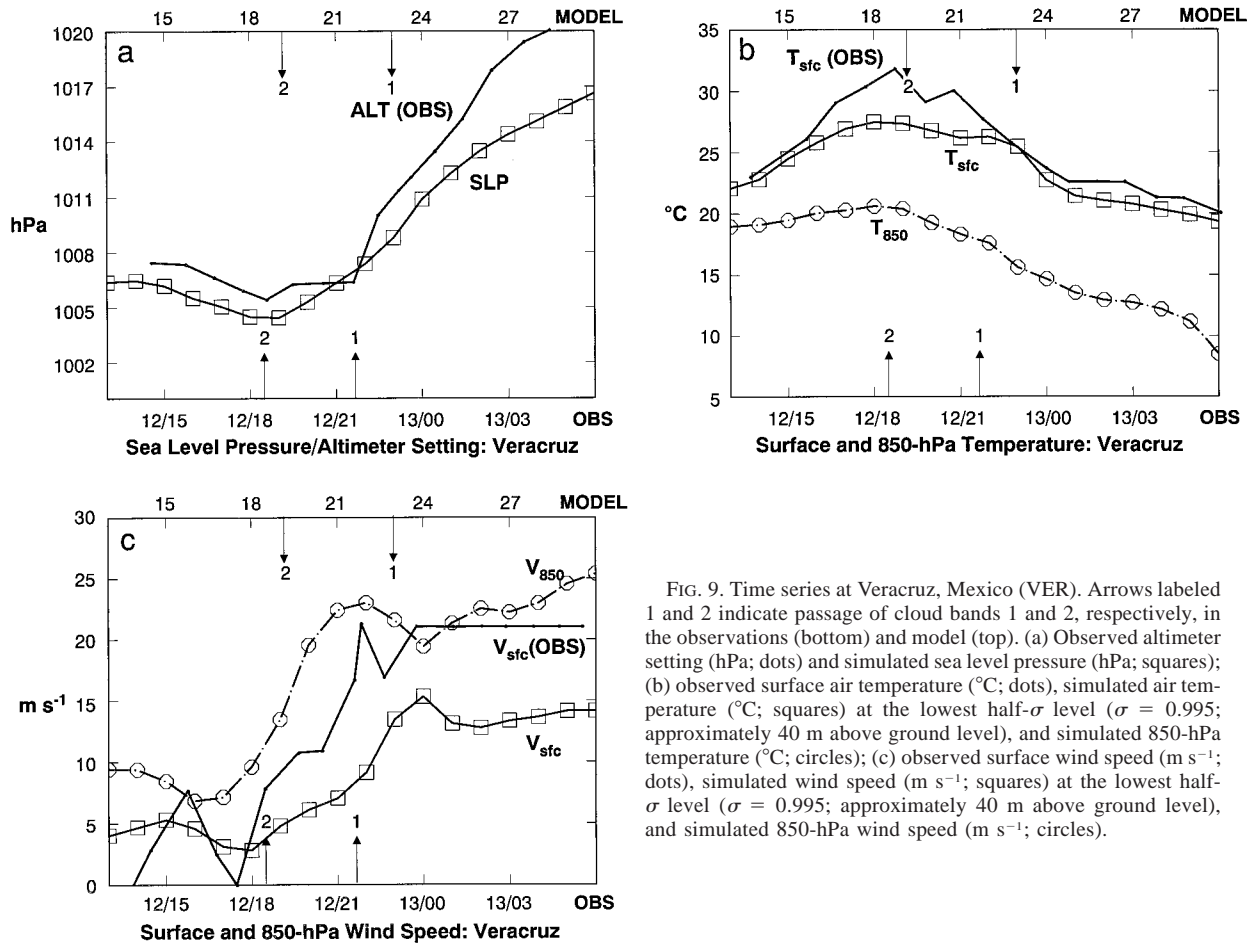


FIG. 9. Time series at Veracruz, Mexico (VER). Arrows labeled 1 and 2 indicate passage of cloud bands 1 and 2, respectively, in the observations (bottom) and model (top). (a) Observed altimeter setting (hPa; dots) and simulated sea level pressure (hPa; squares); (b) observed surface air temperature ($^{\circ}\text{C}$; dots), simulated air temperature ($^{\circ}\text{C}$; squares) at the lowest half- σ level ($\sigma = 0.995$; approximately 40 m above ground level), and simulated 850-hPa temperature ($^{\circ}\text{C}$; circles); (c) observed surface wind speed (m s^{-1} ; dots), simulated wind speed (m s^{-1} ; squares) at the lowest half- σ level ($\sigma = 0.995$; approximately 40 m above ground level), and simulated 850-hPa wind speed (m s^{-1} ; circles).

$$\frac{d}{dt} = \frac{\partial}{\partial t} + u \frac{\partial}{\partial x_p} + v \frac{\partial}{\partial y_p} + \omega \frac{\partial}{\partial p},$$

$$\nabla_p = \mathbf{i} \frac{\partial}{\partial x_p} + \mathbf{j} \frac{\partial}{\partial y_p},$$

and $\mathbf{V} = (u, v, \omega)$ is the total velocity. The subscript p indicates differentiation on an isobaric surface and hereafter will be implicit. Equation (1) can be written

$$F = -\frac{1}{|\nabla\theta|} \left[\underbrace{\frac{\partial\theta}{\partial x} \left(\frac{\partial u}{\partial x} \frac{\partial\theta}{\partial x} + \frac{\partial u}{\partial y} \frac{\partial\theta}{\partial y} \right)}_1 + \underbrace{\frac{\partial\theta}{\partial y} \left(\frac{\partial v}{\partial x} \frac{\partial\theta}{\partial x} + \frac{\partial v}{\partial y} \frac{\partial\theta}{\partial y} \right)}_2 + \underbrace{\frac{\partial\theta}{\partial p} \left(\frac{\partial\omega}{\partial x} \frac{\partial\theta}{\partial x} + \frac{\partial\omega}{\partial y} \frac{\partial\theta}{\partial y} \right)}_3 \right], \quad (2)$$

where terms 1 and 2 represent frontogenesis due to horizontal deformation/divergence and term 3 represents frontogenesis due to tilting of isentropes by horizontal gradients in vertical motion.

The sum of the horizontal frontogenesis terms 1 and 2 in (2), F_{1+2} , also can be expressed in the form developed by Petterssen (1936):

$$F_{1+2} = \frac{1}{2} |\nabla\theta| (E \cos 2\beta - \nabla \cdot \mathbf{V}_H), \quad (3)$$

where E is the resultant deformation, β is the local angle between an isentrope and the axis of dilatation, and $\mathbf{V}_H = (u, v)$ is the horizontal velocity. Note that F_{1+2} consists of two terms; the first term is proportional to the

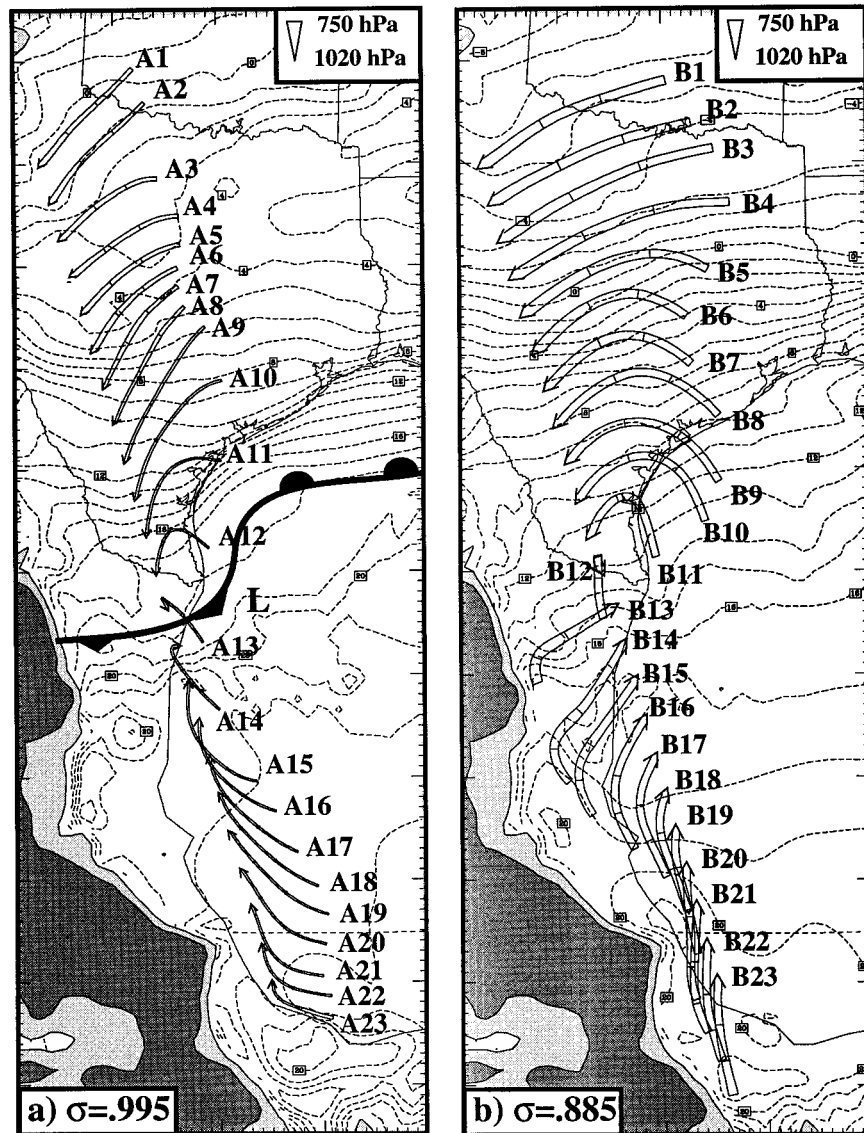


FIG. 10. Nine-hour backward trajectories beginning at 3 h (0300 UTC 12 March 1993) and ending at 12 h (1200 UTC 12 March 1993). Tick marks along trajectory every 3 h. Light (heavy) shading represents topography exceeding 1000 (1500) m in elevation. Surface frontal symbols conventional. (a) Trajectories ending at $\sigma = 0.995$; temperature on $\sigma = 0.995$ (dashed lines every 1°C). Large L indicates position of surface cyclone center. (b) Trajectories ending on $\sigma = 0.885$; temperature at $\sigma = 0.885$ (dashed lines every 1°C).

resultant deformation and the second term is proportional to the horizontal divergence.

As illustrated previously, the formation of the large-scale forward-tilting structure was initiated by the interaction of the surface cold front with the mid- to upper-tropospheric baroclinic zone. In this section, the tilting frontogenesis demonstrates how enhancements of the midtropospheric horizontal potential temperature gradient can occur in association with the lower- to mid-tropospheric ascent along the leading edge of the surface front in order to support the small-scale forward-tilted structure.

At 12 h (Fig. 12a; the location of cross section AB is found in Fig. 3a), much of the cold-frontal region near the surface was associated with deformation/divergence frontogenesis (thick solid lines). Tilting (medium solid lines) contributed to frontogenesis at the leading edge of the front from 950 to 550 hPa, along the equatorward side of the ascent maximum (shaded; presumably associated, in part, with a thermally direct secondary circulation). By 15 h (Fig. 12b), the deformation/divergence frontogenesis along the surface cold front reached its maximum magnitude. Also, the cross-frontal scales of the ascent at the leading edge of the

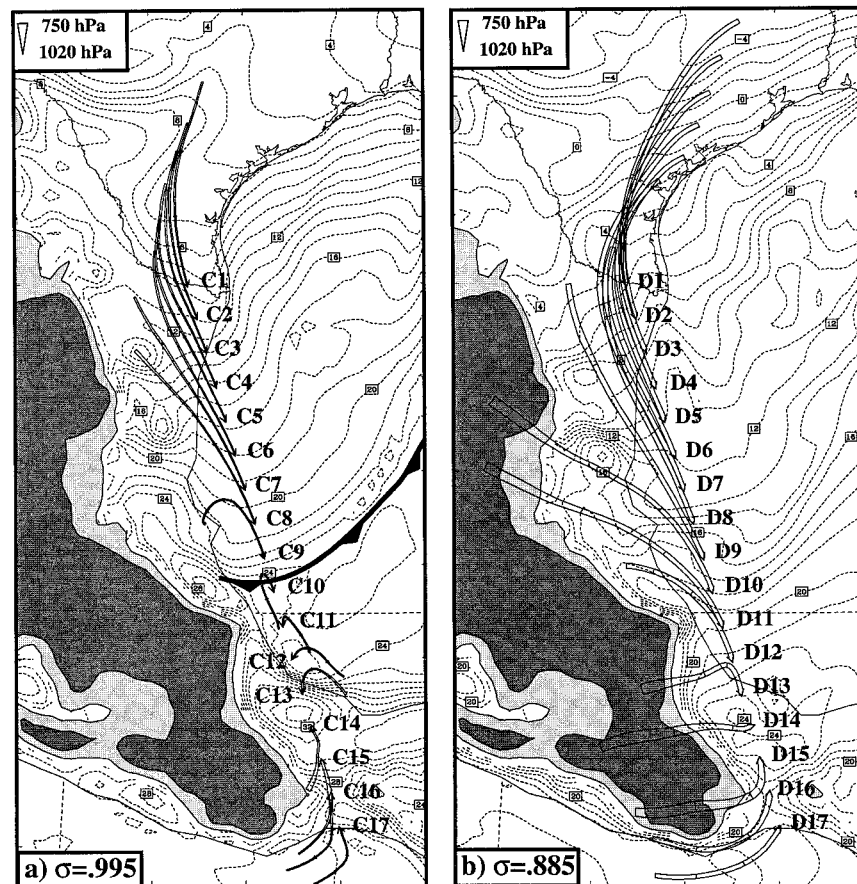


FIG. 11. As in Fig. 10 except beginning at 12 h (1200 UTC 12 March 1993) and ending at 21 h (2100 UTC 12 March 1993).

front and, correspondingly, the regions of tilting frontogenesis have contracted. The arrival of the mid- to upper-tropospheric baroclinic zone into the plane of the cross section is indicated by weak prefrontal ascent and tilting frontogenesis at 850–550 hPa near the leading

TABLE 1. Meteorological variables along trajectory C9 (path of trajectory shown in Fig. 11a). Here p is pressure, q_v is water vapor mixing ratio, RH is relative humidity, θ is potential temperature, and θ_e is equivalent potential temperature.

Hour (h)	p (hPa)	q_v (g kg^{-1})	RH (%)	θ (K)	θ_e (K)
12	994	15.6	93.6	295.1	336.8
13	995	15.5	94.3	294.9	336.5
14	995	15.5	92.1	295.2	336.8
15	996	15.3	87.5	295.8	336.9
16	996	15.5	87.9	295.9	337.5
17	996	15.1	83.4	296.3	336.9
<i>Passage of prefrontal trough</i>					
18	996	13.9	73.2	297.1	334.6
19	996	13.5	69.8	297.3	333.8
<i>Ingestion by frontal zone</i>					
20	996	13.2	71.3	296.7	332.3
21	996	13.5	77.1	295.8	332.1

edge of the cold advection (Fig. 12b). Also, the depth of the circulation associated with cloud band 1 decreased. These changes to the cold-frontal structure result in the regions of strongest horizontal potential temperature gradient (i.e., strongly sloping isentropes when viewed in cross section) collocated with the regions of ascent above the surface cold front and along the mid- to upper-tropospheric baroclinic zone, thereby indicating the importance of the tilting frontogenesis to maintaining and enhancing the small-scale forward tilt of the cold front. At 18 h (Fig. 12c; note the change in horizontal scale from Figs. 12a,b; the location of cross section EF is shown in Fig. 6a), the front became tilted forward even farther on the small scale. Two regions of ascent were apparent: one near the leading edge of the surface front (presumably associated with cloud band 1) and one at 850–750 hPa (presumably associated with cloud band 2). The tilting frontogenesis, likewise, evolved from a single large maximum to two regions at the leading edges of the ascent regions. Note that descent over ascent near the surface frontal position implies 850–900-hPa horizontal divergence. Divergence results in frontolysis [the second term on the right-hand side of (3)] in this area (not shown), weakening

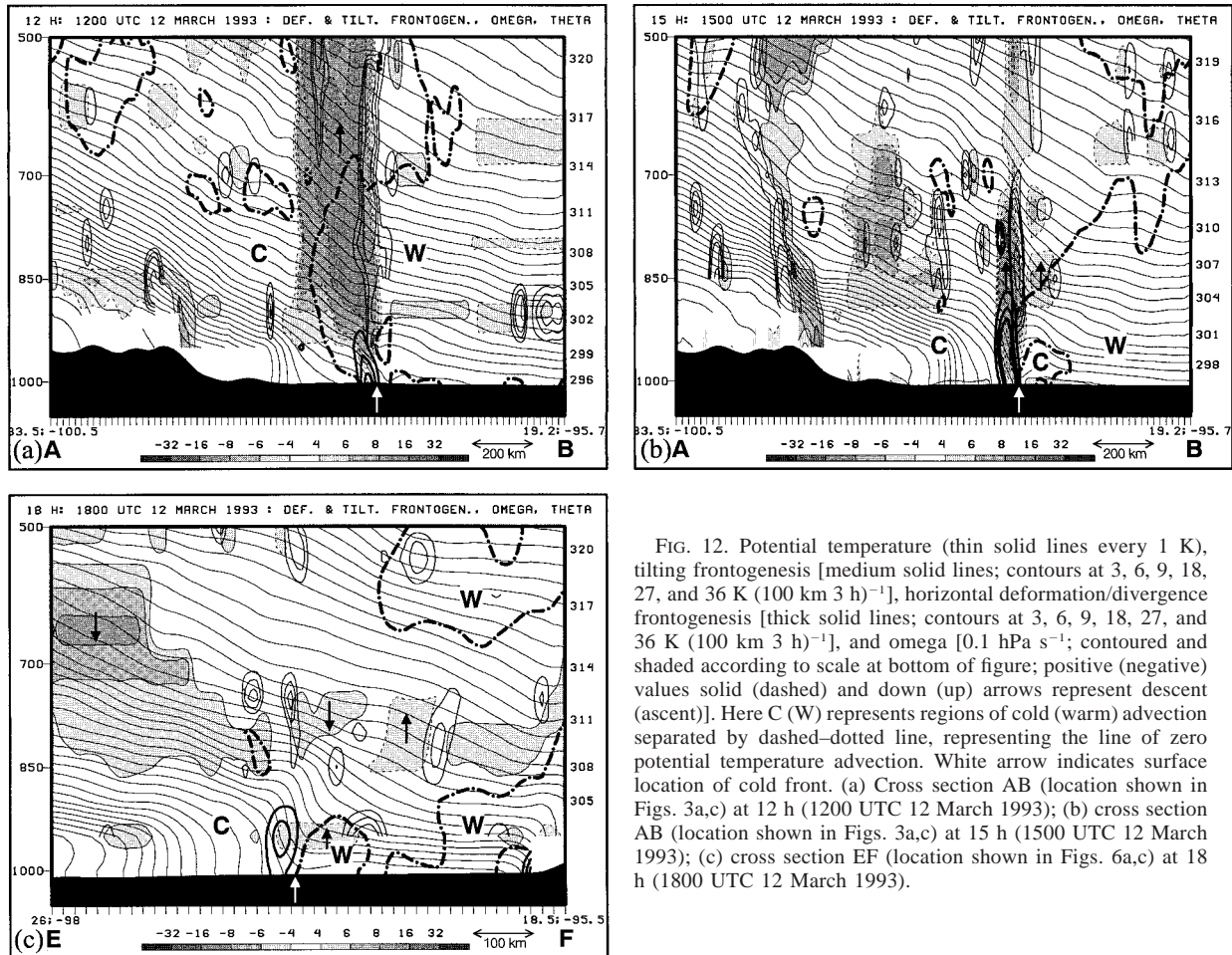


FIG. 12. Potential temperature (thin solid lines every 1 K), tilting frontogenesis [medium solid lines; contours at 3, 6, 9, 18, 27, and 36 $K (100 \text{ km } 3 \text{ h})^{-1}$], horizontal deformation frontogenesis [thick solid lines; contours at 3, 6, 9, 18, 27, and 36 $K (100 \text{ km } 3 \text{ h})^{-1}$], and omega [0.1 hPa s^{-1} ; contoured and shaded according to scale at bottom of figure; positive (negative) values solid (dashed) and down (up) arrows represent descent (ascent)]. Here C (W) represents regions of cold (warm) advection separated by dashed-dotted line, representing the line of zero potential temperature advection. White arrow indicates surface location of cold front. (a) Cross section AB (location shown in Figs. 3a,c) at 12 h (1200 UTC 12 March 1993); (b) cross section AB (location shown in Figs. 3a,c) at 15 h (1500 UTC 12 March 1993); (c) cross section EF (location shown in Figs. 6a,c) at 18 h (1800 UTC 12 March 1993).

the horizontal potential temperature gradient, and the secondary circulation and forcing for ascent for cloud band 1. This weakening of the horizontal potential temperature gradient and dissipation of cloud band 1 led to the dominance of cloud band 2, in agreement with the observations (Fig. 1c).

6. Discussion

In this paper, a mesoscale-model simulation of a forward-tilting cold front in eastern Mexico associated with Superstorm 1993 (SS93) on 12–14 March was examined. This forward-tilting structure comprised two components of differing scale. The large-scale forward tilt formed as an eastward-moving mid- to upper-tropospheric baroclinic zone, extending from the tropopause into the midtroposphere, descended in the lee of the Sierra Madre and interacted with a surface-based cold front arriving from Texas. Embedded within the large-scale forward tilt, a region of stronger horizontal potential temperature gradient was found on smaller scales, maintained by tilting frontogenesis associated with ascent at the leading edge of the surface cold front. Two

cloud bands were also observed with this case. The primary cloud band was likely caused by ascent along the leading edge of the surface cold front. Another region of ascent formed along the leading edge of cold advection in the midtroposphere, likely causing the observed prefrontal cloud band. Eventually, the primary cloud band dissipated, a result of frontolytical divergence associated with the lower-tropospheric subsidence behind the prefrontal cloud band.

The forward-tilting cold-frontal structure in the present case is unusual, but not unique; similar structures have been reported previously in the literature (e.g., section 1). Similar structures, however, do not necessarily imply similar evolutions or dynamics. Therefore, the results from the SS93 case are compared to other forward-tilting cold fronts in section 6a, then placed in a general context for frontal interaction in section 6b.

a. Relationship to other forward-tilting cold fronts

The formation of the forward-tilting cold-frontal structure in the SS93 case by the interaction of a surface cold front and a mid- to upper-tropospheric baroclinic

zone may be similar to a case over the continental United States on 12–14 December 1987 (Schultz and Mass 1993, Fig. 9). In that case, a mid- to upper-tropospheric baroclinic zone interacted with a surface cold front to form a structure that was forward tilting by approximately 200 km from the surface to 800–700 hPa. Another forward-tilting cold-frontal structure was analyzed by Kuo and Reed (1988, Fig. 10a) for the eastern North Pacific cyclone of 13–14 November 1981. While appearing similar to the SS93 and Schultz and Mass (1993) cases with a nose at about 800 hPa, the direct role of the topography of western North America on the land-falling frontal structure of Kuo and Reed (1988) cannot be discounted entirely. [The forward tilt could occur, for example, in the manner discussed by Smith (1982).]

In contrast, the forward-tilting fronts in Shapiro (1984) and Colle and Mass (1995, Fig. 17) appear to be affected by friction, as the nose occurs only a few hundred meters above the earth's surface. Also, there does not appear to be a mid- to upper-tropospheric baroclinic zone involved, and so these cases are not likely to be directly comparable to the SS93 case. For a case of a forward-tilting cold front over the eastern United States, Bedard and Sanders (1978) claimed that the cold front moved faster over a prefrontal inversion than near the surface. This explanation also has been offered for Hardy et al.'s (1973) case of a forward-tilting front (R. Reed 1989, personal communication). Forsdyke (1949, 40) argued that subsidence (and concomitant adiabatic warming) in the cold air and diabatic surface processes acting on midlatitude cold fronts entering the Tropics weaken and slow the equatorward advance of the front at the surface compared to that aloft. Although surface friction, elevated inversions, and diabatic processes were present in the SS93 case, the trajectory and frontogenesis diagnostics used in this study help to affirm that these processes do not appear to play a primary role in the formation of the forward tilt to the cold-frontal structure in the SS93 case. Indeed, an adiabatic simulation of the SS93 cold front (not shown) also produced a forward-tilting front with a structure and evolution comparable to that in the present simulation, indicating that the contribution of diabatic processes to the structure and evolution of this forward-tilting cold front were of secondary importance. Whereas cold fronts can evolve toward a forward-tilting state in a variety of ways, this paper describes only one way in which this can happen (through the interaction of mid- to upper-tropospheric and lower-level baroclinic zones). Evidence for alternative mechanisms that produce forward-tilting fronts has not been as forthcoming in the literature.

b. A general context for frontal interaction

Research in the literature describing the interaction between upper-level and lower-level baroclinic zones is not abundant (Keyser 1986, 253). The studies that do

exist tend to focus on frontal interaction in the lee of the Rocky Mountains, where lower-level frontal structures in land-falling cyclones from the Pacific Ocean are stripped away by the Rockies. Consequently, interaction occurs between the remaining upper-level features and whatever frontal structures occur in the Central Plains. In this section, we explore how the SS93 case compares and contrasts to such previously discussed frontal interactions.

The mid- to upper-tropospheric baroclinic zone originating over the Sierra Madre in the SS93 case appears to resemble what has been termed a *cold front aloft* (e.g., Hobbs et al. 1990; Martin et al. 1990), where a mid- to upper-tropospheric baroclinic zone, associated with cold advection and frontogenesis (the cold front aloft), moves over the Rocky Mountains in association with a 500-hPa trough. Hobbs et al. (1990, 615) suggest that quasigeostrophic ascent associated with the cold front aloft in a region of potential instability downstream of the 500-hPa trough and *in advance* (equatorward) of a surface cold front [see, e.g., Hobbs et al. (1990, their Fig. 16)] can lead to deep moist convection and severe weather [analogous to the vertically coupled jet-front system of Shapiro (1982, Fig. 23)]. In SS93, the mid- to upper-tropospheric baroclinic zone arrived in eastern Mexico *with* the passage of the surface cold front underneath, a situation unlikely to spawn deep moist convection because the stable lower troposphere and large-scale subsidence in the midtroposphere in advance of the front at the surface (e.g., Fig. 6d) would have inhibited strong upward vertical motion. As a result, only the modest cloud bands 1 and 2 occurred [analogous to the vertically uncoupled jet-front system of Shapiro (1982, Fig. 22)], rather than deep moist convection. This evolution may explain the relative lack of precipitation in eastern Mexico associated with the passage of this cold front (Schultz et al. 1997, Figs. 11b–d and 18) when compared to other Mexican cold-frontal cases (T. Bals-Elsholz 1997, personal communication). Therefore, different frontal structures and circulations may result, depending on the timing of the surface and mid- to upper-level baroclinic zones.

One may also envision scenarios where either the surface or the mid- to upper-level baroclinic zone is absent or interaction does not occur. For example, Neiman et al. (1998) analyze a case in which a mid- to upper-tropospheric baroclinic zone (what they term “the Pacific front”) arrived over the United States Central Plains, but there was no surface frontal structure (only a near-surface inversion) with which the mid- to upper-tropospheric baroclinic zone could interact. Elevated convection resulted in a squall line over the southeastern United States along the leading edge of the baroclinic zone aloft. Alternatively, the surface cold front could occur without an interaction with a mid- to upper-tropospheric baroclinic zone; this scenario has been discussed by, for example, Colle and Mass (1995, Fig. 17).

Keyser (1986, 253) advocated further research on the

interaction between surface and mid- to upper-tropospheric baroclinic zones and this investigation represents a contribution to that effort. We envision a spectrum of possible interactions between surface frontal features and mobile mid- to upper-tropospheric baroclinic zones, ranging from a mid- to upper-tropospheric baroclinic zone with no surface front (Neiman et al. 1998) to a surface front with no baroclinic zone aloft (Colle and Mass 1995). In between, the possibility exists for interactions between upper- and lower-level phenomena (e.g., cold fronts aloft, the SS93 cold front) in different environments, which may inhibit or favor deep moist convection and coupling between upper- and lower-tropospheric circulations (e.g., Shapiro 1982, Figs. 22–23). In these instances, the mountains initially maintain the separation between the surface frontal features in the Central Plains and eastern Mexico and the eastward-moving mid- to upper-tropospheric baroclinic zone until interaction. Therefore, depending on the prior weather systems over the Central Plains and eastern Mexico, a variety of structural evolutions and weather patterns can result when mid- to upper-tropospheric baroclinic zones arrive from the west over the Rocky Mountains and the Sierra Madre.

Acknowledgments. This work is a continuation of a graduate-level synoptic-laboratory research project performed by the first author at the University at Albany, State University of New York with Prof. Lance Bosart, Edward Bracken, Dr. Gregory Hakim, Michael Dickinson, Mary Bedrick, and Kevin Tyle. We are deeply indebted to the following individuals for their contributions to this work: Barry Schwartz for providing observations from Central America and Mexico; Prof. Gary Lackmann, Dr. Haig Iskenderian, and Ed Bracken for assistance in obtaining ECMWF analyses and other data; Anton Seimon for allowing access to his surface mesoanalyses of SS93; Teresa Bals-Elsholz for sharing her unpublished research results; Drs. Brian Colle, Charles Doswell, Michael Douglas, John Nielsen-Gammann, David Rust, Fred Sanders, David Stensrud, and an anonymous reviewer for commenting on earlier versions of this manuscript; Dr. Doswell for stimulating discussions on frontal structure and movement; and Dr. Mary Barth, Prof. Lance Bosart, Prof. John Horel, Todd Hutchinson, and Dr. Mark Stoelinga for their advice, contributions, and interest in this project.

We are grateful to ECMWF, the Data Support Section of the Scientific Computing Division of NCAR, and the University of Utah Center for High Performance Computing for providing data and a portion of the computing resources used in this study. Research on this project was partially conducted while the first author was a National Research Council Postdoctoral Research Associate at the National Severe Storms Laboratory. This research was partially supported by the National Science Foundation through Grant ATM-9634191 and NOAA

Grant OGP-526404 to the second author through the University of Utah.

REFERENCES

- Bedard, A. J., Jr., and M. J. Sanders Jr., 1978: Thunderstorm-related wind shear detected at Dulles International Airport using a Doppler acoustic/microwave radar, a monostatic sounder and arrays of surface sensors. *Proc. Conf. on Weather Forecasting and Analysis and Aviation Meteorology*, Silver Spring, MD, Amer. Meteor. Soc., 347–352.
- Berry, F. A., Jr., E. Bollay, and N. R. Beers, 1945: *Handbook of Meteorology*. McGraw-Hill, 1068 pp.
- Bjerknes, J., 1930: Practical examples of polar-front analysis over the British Isles in 1925–6. *Geophys. Mem.*, **5** (10), 1–21 and 28 pp. of figures.
- Bluestein, H. B., 1993: *Synoptic-Dynamic Meteorology in Midlatitudes. Vol. 2, Observations and Theory of Weather Systems*, Oxford University Press, 594 pp.
- Bond, N. A., and R. G. Fleagle, 1985: Structure of a cold front over the ocean. *Quart. J. Roy. Meteor. Soc.*, **111**, 739–759.
- , and M. A. Shapiro, 1991: Research aircraft observations of the mesoscale and microscale structure of a cold front over the eastern Pacific Ocean. *Mon. Wea. Rev.*, **119**, 3080–3094.
- Bosart, L. F., G. J. Hakim, K. R. Tyle, M. A. Bedrick, W. E. Bracken, M. J. Dickinson, and D. M. Schultz, 1996: Large-scale antecedent conditions associated with the 12–14 March 1993 cyclone (“Superstorm ’93”) over eastern North America. *Mon. Wea. Rev.*, **124**, 1865–1891.
- Browning, K. A., 1990: Organization of clouds and precipitation in extratropical cyclones. *Extratropical Cyclones: The Erik Palmén Memorial Volume*, C. W. Newton and E. O. Holopainen, Eds., Amer. Meteor. Soc., 129–153.
- , and T. W. Harrold, 1970: Air motion and precipitation growth at a cold front. *Quart. J. Roy. Meteor. Soc.*, **96**, 369–389.
- , N. M. Roberts, and A. J. Illingworth, 1997: Mesoscale analysis of the activation of a cold front during cyclogenesis. *Quart. J. Roy. Meteor. Soc.*, **123**, 2349–2375.
- Brunt, D., 1934: *Physical and Dynamical Meteorology*. Cambridge University Press, 411 pp.
- Bryan, G. H., and J. M. Fritsch, 1998: Discrete frontal propagation induced by convection. Preprints, *16th Conf. on Weather Analysis and Forecasting*, Phoenix, AZ, Amer. Meteor. Soc., 152–154.
- Charney, J. J., and J. M. Fritsch, 1996: The formation of mesohighs in non-convective environments. Preprints, *15th Conf. on Weather Analysis and Forecasting*, Norfolk, VA, Amer. Meteor. Soc., 242–244.
- Colle, B. A., and C. F. Mass, 1995: The structure and evolution of cold surges east of the Rocky Mountains. *Mon. Wea. Rev.*, **123**, 2577–2610.
- Dickinson, M. J., L. F. Bosart, W. E. Bracken, G. J. Hakim, D. M. Schultz, M. A. Bedrick, and K. R. Tyle, 1997: The March 1993 Superstorm cyclogenesis: Incipient phase synoptic- and convective-scale flow interaction and model performance. *Mon. Wea. Rev.*, **125**, 3041–3072.
- Dudhia, J., 1989: Numerical study of convection observed during the Winter Monsoon Experiment using a mesoscale two-dimensional model. *J. Atmos. Sci.*, **46**, 3077–3107.
- , 1993: A nonhydrostatic version of the Penn State–NCAR mesoscale model: Validation tests and simulation of an Atlantic cyclone and cold front. *Mon. Wea. Rev.*, **121**, 1493–1513.
- Fermor, J. H., 1971: The weather during northers at Kingston, Jamaica. *J. Trop. Geogr.*, **32**, 31–37.
- Flower, W. D., 1931: An analysis of the cold front over Egypt on March 7, 1929. *Quart. J. Roy. Meteor. Soc.*, **57**, 275–287.
- Forsdyke, A. G., 1949: Weather forecasting in tropical regions. *Geophys. Mem.*, **10** (2), 1–47.
- Garratt, J. R., 1988: Summertime cold fronts in southeast Australia—

- Behavior and low-level structure of main frontal types. *Mon. Wea. Rev.*, **116**, 636–649.
- Grell, G. A., J. Dudhia, and D. R. Stauffer, 1994: A description of the fifth-generation Penn State/NCAR Mesoscale Model (MM5). NCAR Tech. Note NCAR/TN-398+STR, 138 pp. [Available from NCAR, P.O. Box 3000, Boulder, CO 80307-3000.]
- Hanstrum, B. N., K. J. Wilson, and S. L. Barrell, 1990a: Prefrontal troughs over Southern Australia. Part I: A climatology. *Wea. Forecasting*, **5**, 22–31.
- , —, and —, 1990b: Prefrontal troughs over Southern Australia. Part II: A case study of frontogenesis. *Wea. Forecasting*, **5**, 32–46.
- Hardy, K. R., R. J. Reed, and G. K. Mather, 1973: Observation of Kelvin–Helmholtz billows and their mesoscale environment by radar, instrumented aircraft, and a dense radiosonde network. *Quart. J. Roy. Meteor. Soc.*, **99**, 279–293.
- Hastenrath, S., 1985: *Climate and Circulation of the Tropics*. D. Reidel, 455 pp.
- Hobbs, P. V., J. D. Locatelli, and J. E. Martin, 1990: Cold fronts aloft and the forecasting of precipitation and severe weather east of the Rocky Mountains. *Wea. Forecasting*, **5**, 613–626.
- Hutchinson, T. A., and H. B. Bluestein, 1998: Prefrontal wind-shift lines in the Plains of the United States. *Mon. Wea. Rev.*, **126**, 141–166.
- Janes, S. A., H. W. Brandli, and J. W. Orndorff, 1976: “The blue line” depicted on satellite imagery. *Mon. Wea. Rev.*, **104**, 1178–1181.
- Kain, J. S., and J. M. Fritsch, 1993: Convective parameterization for mesoscale models: The Kain–Fritsch scheme. *The Representation of Cumulus Convection in Numerical Models*, Meteor. Monogr., No. 24, Amer. Meteor. Soc., 165–170.
- Keyser, D., 1986: Atmospheric fronts: An observational perspective. *Mesoscale Meteorology and Forecasting*, P. S. Ray, Ed., Amer. Meteor. Soc., 216–258.
- Klemp, J. B., and D. R. Durran, 1983: An upper boundary condition permitting internal gravity wave radiation in numerical mesoscale models. *Mon. Wea. Rev.*, **111**, 430–444.
- Knight, D. J., and P. V. Hobbs, 1988: The mesoscale and microscale structure and organization of clouds and precipitation in mid-latitude cyclones. Part XV: A numerical modeling study of frontogenesis and cold-frontal rainbands. *J. Atmos. Sci.*, **45**, 915–930.
- Kocin, P. J., P. N. Schumacher, R. F. Morales Jr., and L. W. Uccellini, 1995: Overview of the 12–14 March 1993 Superstorm. *Bull. Amer. Meteor. Soc.*, **76**, 165–182.
- Kuo, Y.-H., and R. J. Reed, 1988: Numerical simulation of an explosively deepening cyclone in the eastern Pacific. *Mon. Wea. Rev.*, **116**, 2081–2105.
- Locatelli, J. D., J. M. Sienkiewicz, and P. V. Hobbs, 1989: Organization and structure of clouds and precipitation on the mid-Atlantic coast of the United States. Part I: Synoptic evolution of a frontal system from the Rockies to the Atlantic Coast. *J. Atmos. Sci.*, **46**, 1327–1348.
- Martin, J. E., J. D. Locatelli, and P. V. Hobbs, 1990: Organization and structure of clouds and precipitation on the mid-Atlantic coast of the United States. Part III: The evolution of a middle-tropospheric cold front. *Mon. Wea. Rev.*, **118**, 195–217.
- Mass, C. F., and D. M. Schultz, 1993: The structure and evolution of a simulated midlatitude cyclone over land. *Mon. Wea. Rev.*, **121**, 889–917.
- Miller, J. E., 1948: On the concept of frontogenesis. *J. Meteor.*, **5**, 169–171.
- Morales, H. C., 1981: A case study of a dust storm weather situation in the Sudan in April 1973. *Pure Appl. Geophys.*, **119**, 658–676.
- Neiman, P. J., P. T. May, B. B. Stankov, and M. A. Shapiro, 1991: Radio acoustic sounding system observations of an arctic front. *J. Appl. Meteor.*, **30**, 881–892.
- , F. M. Ralph, M. A. Shapiro, B. F. Smull, and D. Johnson, 1998: An observational study of fronts and frontal mergers over the continental United States. *Mon. Wea. Rev.*, **126**, 2521–2554.
- Newton, C. W., 1950: Structure and mechanism of the prefrontal squall line. *J. Meteor.*, **7**, 210–222.
- , 1963: Dynamics of severe convective storms. *Severe Local Storms*, Meteor. Monogr., No. 5, Amer. Meteor. Soc., 33–58.
- Palmer, C. E., 1951: Tropical meteorology. *Compendium of Meteorology*, T. F. Malone, Ed., Amer. Meteor. Soc., 859–880.
- Petterssen, S., 1936: Contribution to the theory of frontogenesis. *Geophys. Publ.*, **11** (6), 1–27.
- Sanders, F., 1955: An investigation of the structure and dynamics of an intense surface frontal zone. *J. Meteor.*, **12**, 542–552.
- , 1983: Observations of fronts. *Mesoscale Meteorology—Theories, Observations and Models*, D. K. Lilly and T. Gal-Chen, Eds., D. Reidel, 175–203.
- , 1998: A proposed method of surface map analysis. Preprints, *16th Conf. on Weather Analysis and Forecasting*, Phoenix, AZ, Amer. Meteor. Soc., 214–217.
- , and C. A. Doswell III, 1995: A case for detailed surface analysis. *Bull. Amer. Meteor. Soc.*, **76**, 505–521.
- Schultz, D. M., and C. F. Mass, 1993: The occlusion process in a midlatitude cyclone over land. *Mon. Wea. Rev.*, **121**, 918–940.
- , W. E. Bracken, L. F. Bosart, G. J. Hakim, M. A. Bedrick, M. J. Dickinson, and K. R. Tyle, 1997: The 1993 Superstorm cold surge: Frontal structure, gap flow, and tropical impact. *Mon. Wea. Rev.*, **125**, 5–39; Corrigendum, **125**, 662.
- Seaman, N. L., 1987: Program TRAJEC: Documentation and user’s guide. PSU-NWPLIB-0010-87, 95 pp. [Available from Department of Meteorology, The Pennsylvania State University, University Park, PA 16802.]
- Shapiro, M. A., 1982: Mesoscale weather systems of the central United States. CIRES/NOAA Tech. Rep., 78 pp. [Available from Cooperative Institute for Research in Environmental Sciences, University of Colorado/NOAA, Boulder, CO 80309.]
- , 1984: Meteorological tower measurements of a surface cold front. *Mon. Wea. Rev.*, **112**, 1634–1639.
- , and D. Keyser, 1990: Fronts, jet streams, and the tropopause. *Extratropical Cyclones: The Erik Palmén Memorial Volume*, C. W. Newton and E. O. Holopainen, Eds., Amer. Meteor. Soc., 167–191.
- Smith, R. B., 1982: A differential advection model of orographic rain. *Mon. Wea. Rev.*, **110**, 306–309.
- Steenburgh, W. J., and C. F. Mass, 1994: The structure and evolution of a simulated Rocky Mountain lee trough. *Mon. Wea. Rev.*, **122**, 2740–2761.
- , D. M. Schultz, and B. A. Colle, 1998: The structure and evolution of gap outflow over the Gulf of Tehuantepec, Mexico. *Mon. Wea. Rev.*, **126**, 2673–2691.
- Tepper, M., 1950: A proposed mechanism of squall lines: The pressure jump line. *J. Meteor.*, **7**, 21–29.
- Trewartha, G. T., 1966: *The Earth’s Problem Climates*. University of Wisconsin Press, 334 pp.
- Zhang, D., and R. A. Anthes, 1982: A high-resolution model of the planetary boundary layer—Sensitivity tests and comparisons with SESAME-79 data. *J. Appl. Meteor.*, **21**, 1594–1609.